Effects of Source and Load Impedance on the Insertion Loss of Expansion Chamber Hydraulic Noise Suppressors

Fan Yang and Jianpin Zhang

Ministry of Education Key Laboratory of Testing Technology for Manufacturing Process, Southwest University of Science and Technology, Mianyang, Sichuan 621000, China. E-mail: yyff90@foxmail.com

Xuepeng Cao

Institute of Hydromechtronics, Chang'an University, Xi'an, Shanxi 710064, China.

Bin Deng

Engineering Research Center of Advanced Driving Energy-saving Technology of Ministry of Education, Department of Mechanical Engineering, Southwest Jiaotong University, Chengdu, Sichuan 610000, China.

(Received 8 April 202; accepted 19 November2022)

Currently, the acoustical performance of hydraulic noise attenuators is usually measured in terms of insertion loss (IL) and transmission loss (TL). Compared with the TL, experimental measurements of IL appear to be easier, however, the acquisition of source and load impedance for theoretical IL seems to be time-consuming and costly. Considering that the analogy between electrical system variables and fluidic ones is complete, well-established electrical circuit representations could be used for hydraulic systems using expansion chamber configurations as the hydraulic suppressors. Utilizing the Thevenin theorem and Norton theorem in the electrical network theory, two types of pressure oscillation source representations are equivalent insofar as the suppressors are concerned and then the expression for IL could be simplified. Finally, through the experimental measurements of the IL, the most suitable electrical representation would be selected. By implementing this method, the measurements of source impedance and load impedance tend to be avoided, which appears to be an attractive approach.

NOMENCLATURE

p	pressure oscillation
k	wave number
j	imaginary unit
ω	angular frequency
c_0	sound speed
f	frequency
x	axial coordinate
t	time
v	particle velocity
ρ_0	density of the medium
S	cross-sectional area
Q	mass velocity
Y	characteristic impedance
Z	acoustical impedance
R	real component of the acoustic impedance

1. INTRODUCTION

A hydraulic line between a pump and a load comes under much stress since a huge pressure oscillation in the hydraulic system decreases reliability.[1,2] To attenuate the pulsation, installing pressure dampers tends to be an effective method.[3,4] Compared with the Helmholtz resonator and T-pipe, the operating band of an expansion chamber attenuator (ECA) seems to be widest,[5] therefore, an ECA is usually used to damp fluid-borne noise and pulsating flows.

The objective of the present work is to study the IL of a hydraulic system using expansion chambers as the suppressors. To get the theoretical IL, load impedance and source impedance are also needed, in addition to the four-pole parameters of the hydraulic system. However, the experimental measurement of sound source impedance not only requires corresponding testing instruments and equipment but also costs time and high cost.[6] Considering that the electrical circuit representations for an acoustic system seem to be complete, the Thevenin theorem and Norton theorem in the electrical network theory could be used to make two types of source representations for the hydraulic pump, which could simplify the expression of the theoretical IL. Although the results obtained by using these models appear to be quite different, combined with experimental measurements, the most suitable model could be finally determined.

2. ANALYTICAL APPROACH

2.1. Transfer Matrix Method

In the ideal case of a rigid duct filled with stationary fluid, small-amplitude waves travel as plane waves.[6,7] The solution to the plane wave equation can be expressed:

$$\frac{\delta^2 p}{\delta x^2} - \frac{1}{c_0^2}\frac{\delta^2 p}{\delta t^2}; \tag{1}$$

$$p(x,t) = Ae^{j(\omega t - kx)} + Be^{j(\omega t + kx)}; \tag{2}$$

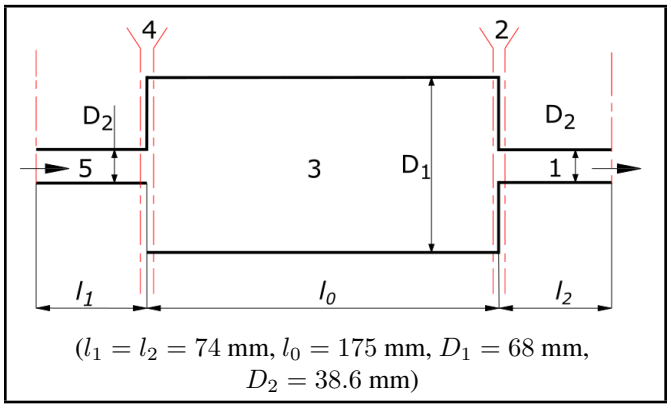

($l_1 = l_2 = 74$ mm, $l_0 = 175$ mm, $D_1 = 68$ mm, $D_2 = 38.6$ mm)

Figure 1. Simple expansion chamber (SEC) attenuator.

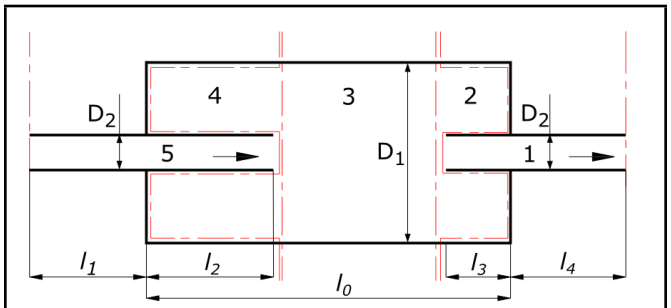

($l_0 = 175$ mm, $l_1 = l_4 = 74$ mm, $l_2 = l_{0/2}$, $l_3 = l_{0/4}$, $D_2 = 38.6$ mm, $D_1 = 68$ mm)

Figure 2. Extended-tube expansion chamber (ETEC) attenuator.

$$Q(x,t) = \frac{1}{Y}\left[Ae^{j(\omega t - kx)} - Be^{j(\omega t + kx)}\right]. \tag{3}$$

The transfer matrix method (TMM) based on the plane wave theory has been known for a long time and tends to be the most widely used approach owing to the fast calculating speed.[8,9] The basic idea of this method is to divide the hydraulic noise suppressor into several basic acoustic units, and then the relationship between the import and export of each unit is represented by a transfer matrix, which could be expressed as:

$$\begin{bmatrix} p_n \\ Q_n \end{bmatrix} = \begin{bmatrix} A_{11} & A_{12} \\ A_{21} & A_{22} \end{bmatrix} \begin{bmatrix} p_{n-1} \\ Q_{n-1} \end{bmatrix}; \tag{4}$$

where $[p_n\ Q_n]$ is called the state vector at the upstream point n, $[p_{n-1}\ Q_{n-1}]$ is the state vector at the downstream point $n-1$, and A_{11}, A_{12}, A_{21}, and A_{22} are the four-pole parameters. The TMM consists in writing down the Eq. (4) of each of the tubular elements and the various element junctions and solving the same simultaneously to evaluate the IL or TL.

2.2. Acoustic Unit Division

Two different kinds of circular concentric expansion chambers are studied in this paper, and their acoustic units are shown in Figs. 1 and 2.

It can be observed from Figs. 1 and 2 that all the elements could be represented by three basic types, uniform tubes, lumped in-line elements, and lumped shunt elements, as shown in Fig. 3.

The transfer matrices of the uniform tube, in-line lumped element, and the shunt lumped element can be written as:

$$\begin{bmatrix} p_n \\ Q_n \end{bmatrix} = \begin{bmatrix} \cos kl_n & jY_n \sin kl_n \\ j/Y_n \sin kl_n & \cos kl_n \end{bmatrix} \begin{bmatrix} p_{n-1} \\ Q_{n-1} \end{bmatrix}; \tag{5}$$

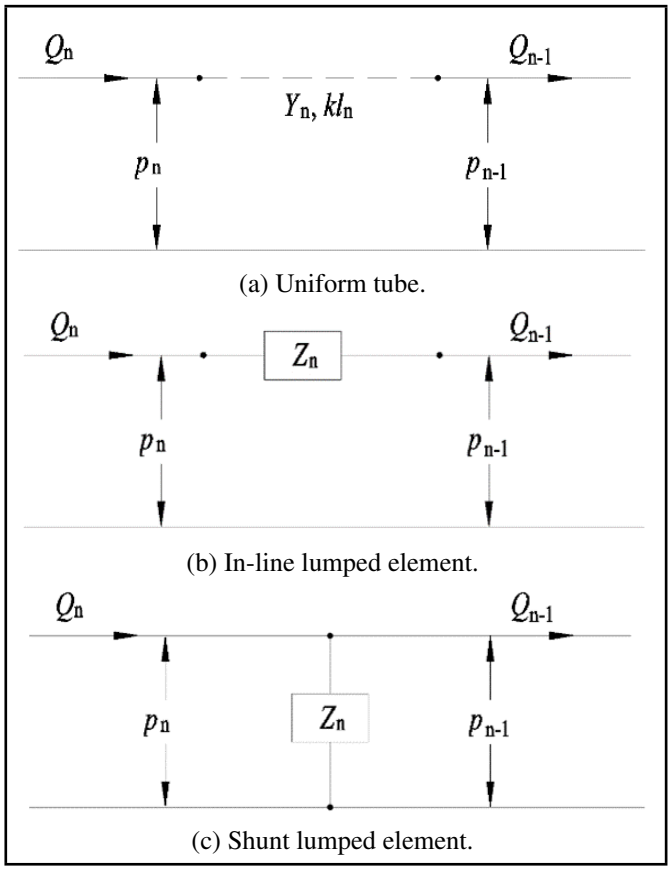

Figure 3. Three basic element types in an equivalent circuit.

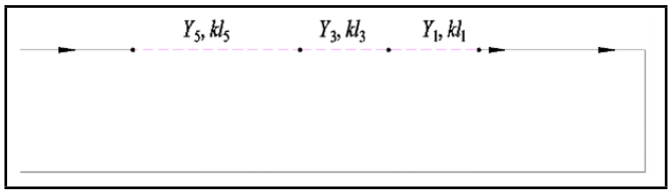

Figure 4. Equivalent circuit for the SEC attenuator.

$$\begin{bmatrix} p_n \\ Q_n \end{bmatrix} = \begin{bmatrix} 1 & Z_n \\ 0 & 1 \end{bmatrix} \begin{bmatrix} p_{n-1} \\ Q_{n-1} \end{bmatrix}; \tag{6}$$

$$\begin{bmatrix} p_n \\ Q_n \end{bmatrix} = \begin{bmatrix} 1 & 0 \\ 1/Z_n & 1 \end{bmatrix} \begin{bmatrix} p_{n-1} \\ Q_{n-1} \end{bmatrix}; \tag{7}$$

The acoustic impedance Z_n is given by Eqs. (2) and (3), that is,[10–12]

$$Z_n = \frac{P_n}{Q_n} = Y_n \frac{\zeta_{end} \cos kl_n + jY_n \sin kl_n}{j\zeta_{end} \sin kl_n + Y_n \cos kl_n} \tag{8}$$

$$\lim_{\zeta_{end} \to \infty} Z_n = -jY_n \cot kl_n; \tag{9}$$

where ζ_{end} is the normal impedance.

Figures 1 and 2 show line diagrams of SEC and ETEC dampers consisting of five elements ($n = 5$). The equivalent circuits are shown in Figs. 4 and 5.

The damper's acoustic attenuation performance (AAP) is measured in terms of IL here. The expression for IL can be expressed as:[10–12]

$$IL = 20 \lg \left[\left(\frac{\rho_{0,2} R_{0,1}}{\rho_{0,1} R_{0,2}} \right)^{1/2} \left| \frac{p_s}{(Z_s + Z_{0,1}) Q_0} \right| \right]; \tag{10}$$

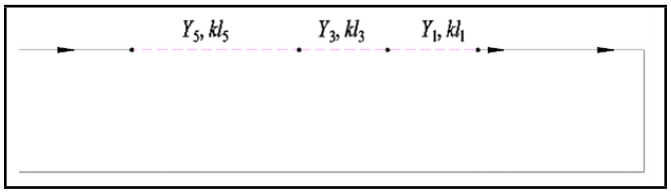

Figure 5. Equivalent circuit for the ETEC attenuator.

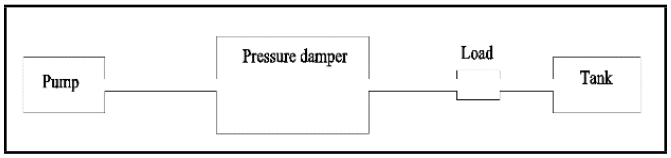

Figure 6. Schematic hydraulic diagram of the test.

where subscripts 1 and 2 denote hydraulic systems without damper and with damper, $Z_{0,1}$ and $Z_{0,2}$ are the corresponding load impedance, $R_{0,1}$ and $R_{0,2}$ are the real components of the impedance $Z_{0,1}$ and $Z_{0,2}$, Z_s is the internal impedance of the source, p_s is the pulsating pressure and Q_0 is the mass velocity flowing through the load.

On assuming that the load used in this hydraulic system is a servo valve and it could be seen as laminar flow resistance,[10–12] which means that the expression, $Z_{0,1} = Z_{0,2} = R_{0,1} = R_{0,2} = R$, could be obtained, as is generally the case, and noting that the medium density $\rho_{0,1}$ would be equal to $\rho_{0,2}$. Eq. (10) for IL becomes:

$$IL = 20 \lg \left[\left| \frac{Z_s}{(Z_s + R)} \right| \left| \frac{Q_s}{Q_0} \right| \right]. \tag{11}$$

From Eq. (11), a conclusion that the source impedance (hydraulic pumps) and load impedance have effects on the theoretical IL can be drawn. However, the experimental measurements for the impedance seem to be costly and time-consuming. Considering that the analogy between electrical system variables and acoustical ones is complete, the well-established electrical circuit representation for the hydraulic system using the suppressors could be used.

2.3. Electrical Circuit Representations of Hydraulic Systems

A hydraulic system consists of the whole structure from the pump to the load, as shown in Fig. 6.

Making use of the Thevenin theorem and Norton theorem in the electrical network theory,[13] two types of source representations are shown in Fig. 7.

According to the Figs. 4 and 7, two kinds of transfer matrix relations can be given by:

$$\begin{bmatrix} p_s \\ Q_s \end{bmatrix} = \begin{bmatrix} 1 & Z_s \\ 0 & 1 \end{bmatrix} \begin{bmatrix} \cos kl_5 & jY_5 \sin kl_5 \\ j/Y_5 \sin kl_5 & \cos kl_5 \end{bmatrix} \begin{bmatrix} 1 & 0 \\ 0 & 1 \end{bmatrix} \begin{bmatrix} \cos kl_3 & jY_3 \sin kl_3 \\ j/Y_3 \sin kl_3 & \cos kl_3 \end{bmatrix} \times \begin{bmatrix} 1 & 0 \\ 0 & 1 \end{bmatrix} \begin{bmatrix} \cos kl_1 & jY_1 \sin kl_1 \\ j/Y_1 \sin kl_1 & \cos kl_1 \end{bmatrix} \begin{bmatrix} 1 & Z_0 \\ 0 & 1 \end{bmatrix} \begin{bmatrix} 0 \\ Q_0 \end{bmatrix}; \tag{12}$$

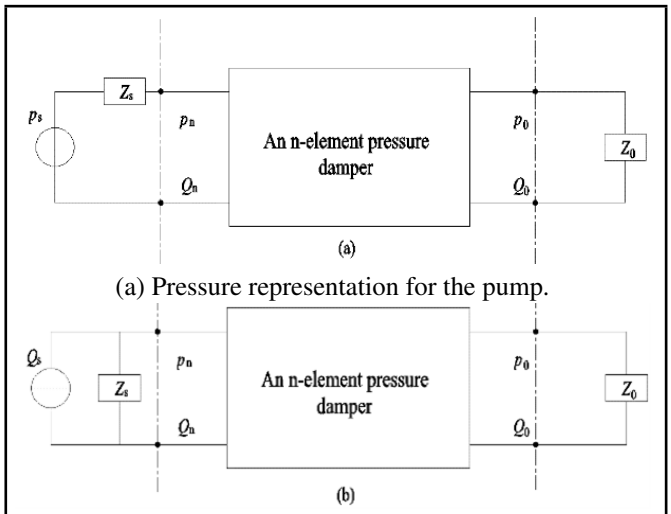

(a) Pressure representation for the pump.

(b) Velocity representation for the pump.

Figure 7. Schematic diagram of the electrical circuit representation of the hydraulic system.

$$\begin{bmatrix} p_s \\ Q_s \end{bmatrix} = \begin{bmatrix} 1 & 0 \\ 1/Z_s & 1 \end{bmatrix} \begin{bmatrix} \cos kl_5 & jY_5 \sin kl_5 \\ j/Y_5 \sin kl_5 & \cos kl_5 \end{bmatrix} \begin{bmatrix} 1 & 0 \\ 0 & 1 \end{bmatrix} \begin{bmatrix} \cos kl_3 & jY_3 \sin kl_3 \\ j/Y_3 \sin kl_3 & \cos kl_3 \end{bmatrix} \times \begin{bmatrix} 1 & 0 \\ 0 & 1 \end{bmatrix} \begin{bmatrix} \cos kl_1 & jY_1 \sin kl_1 \\ j/Y_1 \sin kl_1 & \cos kl_1 \end{bmatrix} \begin{bmatrix} 1 & Z_0 \\ 0 & 1 \end{bmatrix} \begin{bmatrix} 0 \\ Q_0 \end{bmatrix}; \tag{13}$$

According to the Figs. 5 and 7, two kinds of relations also could be written as:

$$\begin{bmatrix} p_s \\ Q_s \end{bmatrix} = \begin{bmatrix} 1 & Z_s \\ 0 & 1 \end{bmatrix} \begin{bmatrix} \cos kl_5 & jY_5 \sin kl_5 \\ j/Y_5 \sin kl_5 & \cos kl_5 \end{bmatrix} \begin{bmatrix} 1 & 0 \\ 1/Z_4 & 1 \end{bmatrix} \begin{bmatrix} \cos kl_3 & jY_3 \sin kl_3 \\ j/Y_3 \sin kl_3 & \cos kl_3 \end{bmatrix} \times \begin{bmatrix} 1 & 0 \\ 1/Z_2 & 1 \end{bmatrix} \begin{bmatrix} \cos kl_1 & jY_1 \sin kl_1 \\ j/Y_1 \sin kl_1 & \cos kl_1 \end{bmatrix} \begin{bmatrix} 1 & Z_0 \\ 0 & 1 \end{bmatrix} \begin{bmatrix} 0 \\ Q_0 \end{bmatrix}; \tag{14}$$

$$\begin{bmatrix} p_s \\ Q_s \end{bmatrix} = \begin{bmatrix} 1 & 0 \\ 1/Z_s & 1 \end{bmatrix} \begin{bmatrix} \cos kl_5 & jY_5 \sin kl_5 \\ j/Y_5 \sin kl_5 & \cos kl_5 \end{bmatrix} \begin{bmatrix} 1 & 0 \\ 1/Z_4 & 1 \end{bmatrix} \begin{bmatrix} \cos kl_3 & jY_3 \sin kl_3 \\ j/Y_3 \sin kl_3 & \cos kl_3 \end{bmatrix} \times \begin{bmatrix} 1 & 0 \\ 1/Z_2 & 1 \end{bmatrix} \begin{bmatrix} \cos kl_1 & jY_1 \sin kl_1 \\ j/Y_1 \sin kl_1 & \cos kl_1 \end{bmatrix} \begin{bmatrix} 1 & Z_0 \\ 0 & 1 \end{bmatrix} \begin{bmatrix} 0 \\ Q_0 \end{bmatrix}; \tag{15}$$

2.4. Source And Load Impedance Simplified Models

According to Fig. 7 (a), for the hypothetical case, $p_s/Q_s >> Z_s$, the constant pressure source working condition ($Z_s \approx 0$) can be obtained. Then, the matrix of the source impedance in Eqs. (12) and (14) seem to be simplified as follows:

$$\begin{bmatrix} 1 & Z_s \\ 0 & 1 \end{bmatrix} \Longrightarrow \begin{bmatrix} 1 & 0 \\ 0 & 1 \end{bmatrix}. \tag{16}$$

For Fig. 7 (b), considering the ideal case, $p_s/Q_s << Z_s$, the constant velocity source working condition ($Z_s \Longrightarrow \infty$) can

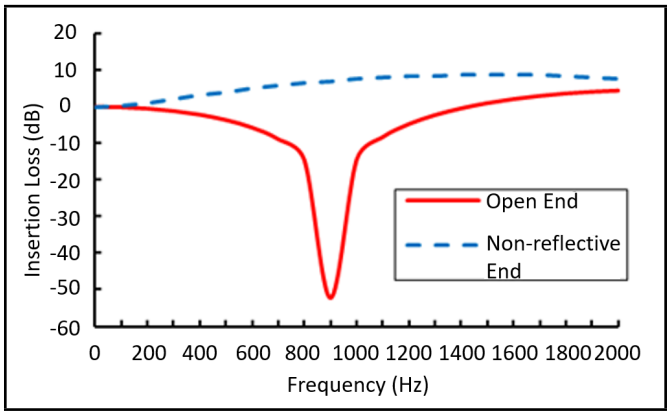

Figure 8. Load impedance of the SEC attenuator.

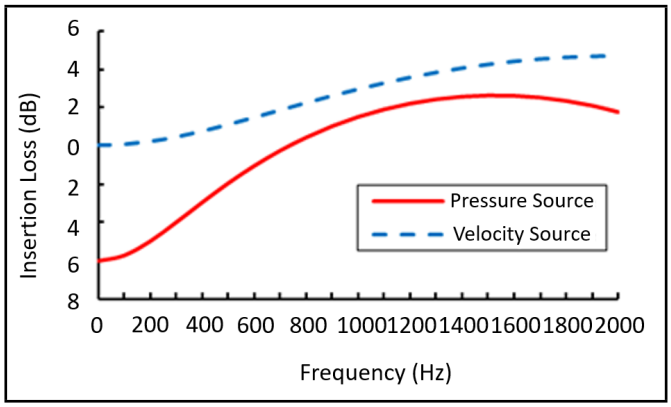

Figure 9. Source representations for the SEC attenuator.

be obtained. The matrix of the source impedance in Eqs. (13) and (15) can also be expressed as:

$$\begin{bmatrix} 1 & 0 \\ 1/Z_s & 1 \end{bmatrix} \Longrightarrow \begin{bmatrix} 1 & 0 \\ 0 & 1 \end{bmatrix}. \tag{17}$$

Another hypothetical case is called the non-reflective working condition, which means that $Z_s = Y_s$ and $Z_0 = Y_0$. Additionally, the condition $Y_s = Y_0$ simply requires the area of the upstream pipe to equal that of the downstream pipe, which is true in this paper. As a result, the matrix of the source impedance in Fig. 7 can be separately expressed as:

$$\begin{bmatrix} 1 & Z_s \\ 0 & 1 \end{bmatrix} \Longrightarrow \begin{bmatrix} 1 & Y_0 \\ 0 & 1 \end{bmatrix}; \tag{18}$$

$$\begin{bmatrix} 1 & 0 \\ 1/Z_s & 1 \end{bmatrix} \Longrightarrow \begin{bmatrix} 1 & 0 \\ 1/Y_0 & 1 \end{bmatrix}. \tag{19}$$

3. EFFECTS OF SOURCE AND LOAD IMPEDANCE

From the Eqs. (11) and (16) - (19), it is possible that the source and load impedance have effects on the IL. As the frequency range of interest is below 2000 Hz, the maximum frequency in calculation here is set to be 2000 Hz. For the boundary conditions, open-end ($Z_0 = 0$) and the non-reflective end ($Z_0 = Y_0$) are considered.

3.1. SEC Attenuator Insertion Loss

Figure 8 shows the effects of the load impedance on the IL when the pump is seen as the constant source, constant pressure source ($Z_s \approx 0$), or constant velocity source ($Z_s \Longrightarrow \infty$).

Figure 9 shows the effects of different source representations (pressure source and velocity source) on the IL of the SEC attenuator when the non-reflective working condition ($Z_s = Y_s = Z_0 = Y_0$) is considered.

Figures 8 and 9 show that using different kinds of load impedance and source representations for the SEC attenuator would have diverse IL curves.

3.2. ETEC Attenuator Insertion Loss

Figure 10 shows the effects of the load impedance on the IL of the ETEC attenuator.

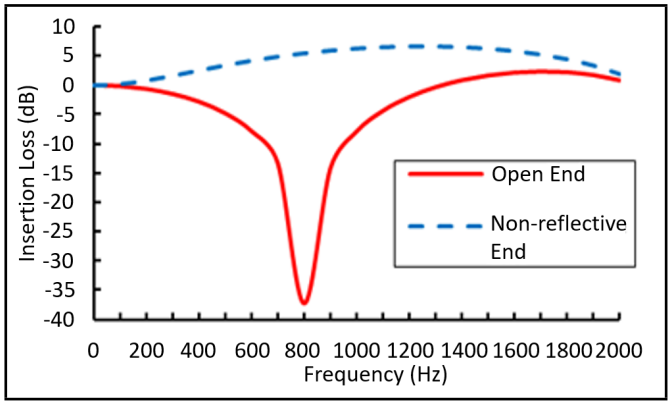

Figure 10. Load impedance of the ETEC attenuator.

Figure 11 shows the effects of different source representations on the IL of the ETEC attenuator.

Figures 10 and 11 show that for the ETEC attenuator, using different kinds of load impedance and source representations also has diverse IL curves. Therefore, to decide which curves could represent the AAP of these suppressors, the experimental measurement for the IL should be conducted.

4. EXPERIMENT

To validate these analytical model predictions, an SEC and an ETEC were fabricated and tested. The relevant dimensions of the suppressors are found in Figs. 1 and 2. The hydraulic fluid used in these tests has density ρ_0 = 866 kg/m^3 and sound speed c_0 = 1400 m/s.[14]

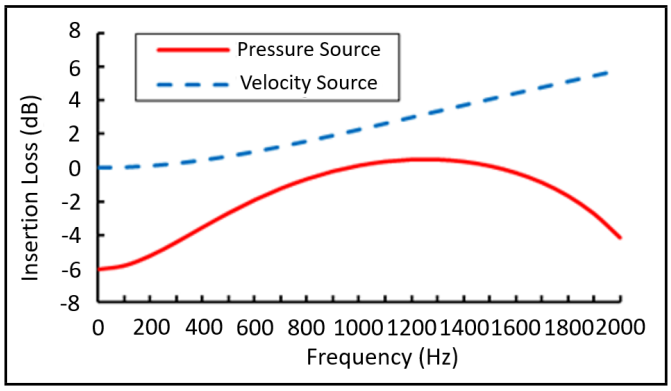

Figure 11. Source representations for the ETEC attenuator.

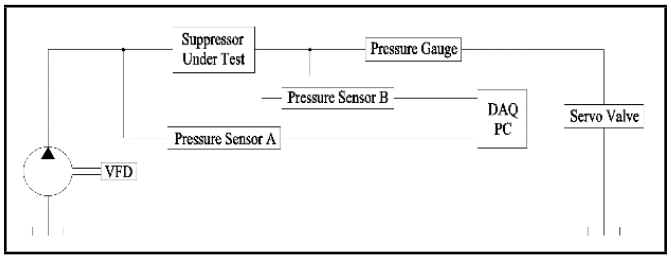

Figure 12. Schematic diagram of the suppressor under test.

4.1. Test Setup

A schematic of the test rig is shown in Fig. 12. The inner radius of the pipes is such that only plane waves may propagate: the cut-on frequency for the first radial mode is much higher than the frequency range of interest (2 kHz). The pump is a 9-piston axial piston pump, the displacement is 28 mL/r, the rated speed is 4750 r/min and the rated working pressure is 20 MPa, driven by a variable-speed ac motor, Y280S-4-B3. A variable-frequency drive (VFD) powers the motor. The analog signals from the high-bandwidth piezoelectric pressure transducers, CYY28, are then digitized by a 16-channel National Instruments data acquisition board, USB5935, whose maximum sampling rate could reach 500 kHz. The pressure range, sensitivity and frequency response of the CYY28 are 50 MPa, 0.25 % and 10 kHz respectively.

A relief valve is located downstream of the damper under test. This valve is used to load the system to a given static pressure. The experimental devices are shown in Fig. 13.

4.2. Test Method

According to the test setup shown in Fig. 12, the specific testing process can be expressed as:

1. The system was a load to 13 MPa, by regulating the servo valve;

2. The VFD was regulated to generate different pump speeds and the pressure data from sensor B were collected;

3. A circular pipe was substituted for the suppressor under test. Then, data from sensor B were collected under the same working conditions; and,

4. Using the spectrum analysis, the experimental values of IL were obtained.

4.3. Results

Figure 14 represents the experimental measurements of the IL of the SEC and ETEC dampers.

As for the SEC damper, comparing the Figs. 8, 9, and 14 a, the most suitable analytical model is the non-reflective end, as shown in Fig. 15.

Figure 16 shows that for the ETEC damper, comparing the Figs. 10, 11, and 14 b, the most suitable model is also the non-reflective end.

Figures 15 and 16 show that for the SEC and ETEC suppressors, applying experimental measurements of the IL could finally screen the most suitable analytical model.

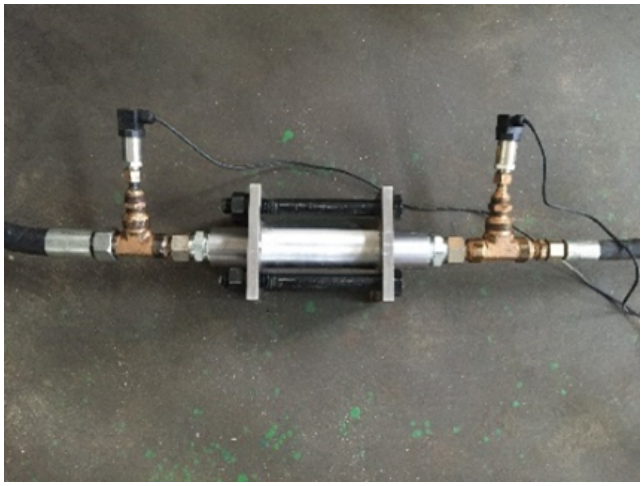

(a) Photograph of the expansion chamber.

(b) Photograph of the pressure sensors.

Figure 13. Photographs of the experimental devices.

5. CONCLUSIONS

The calculation of theoretical IL of the hydraulic suppressors needs the values of source and load impedance. However, the measurements for the impedance tend to be difficult and time-consuming. To predict the IL of the SEC and ETEC suppressors, this paper used the Thevenin theorem and Norton theorem in the electrical theory to make two different source representations (pressure representation and velocity representation) for the hydraulic pump regarding the servo valve which is used as the load as the laminar resistance. The results show that in the frequency range of 2000 Hz, different representations for the source and various values of the load impedance (open-end and non-reflective end) have diverse IL curves. However, combined with the experimental measurements, the most suitable source representation and load impedance could be screened. To conclude, using the electrical circuit representations for the hydraulic pump and valve used as loads could avoid directly measuring the source and load impedance. Then, according to the experimental values of IL, the ideal model would be screened, which is an appealing method.

REFERENCES

[1] Kojima, E., Ichiyanagi, T. Research on pulsation attenuation characteristics of silencers in practical fluid power sys-

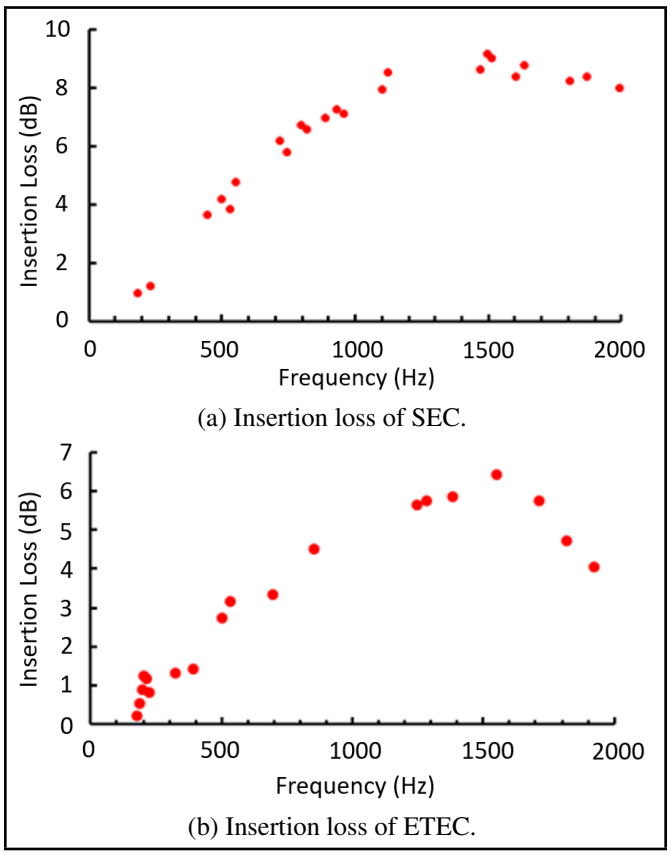

Figure 14. Experimental measurements of the dampers.

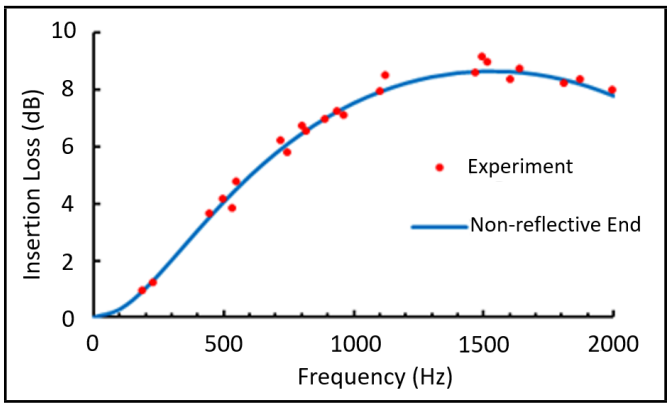

Figure 15. Comparative results for the Insertion loss of the SEC suppressor.

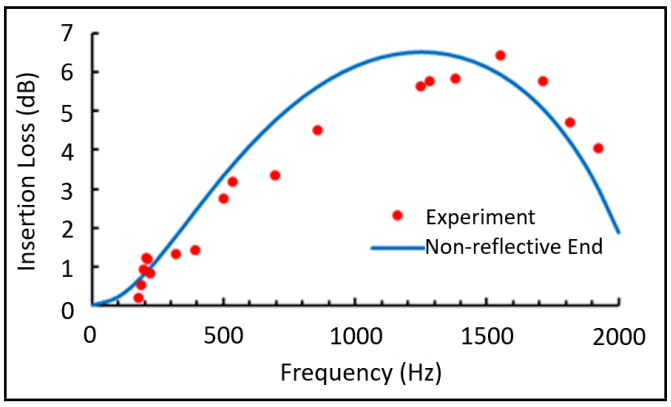

Figure 16. Comparative results for the Insertion loss of the ETEC suppressor.

tems[J], *International Journal of Fluid Power*, **1**(2), 29-38, (2000). https://doi.org/10.1080/14399776.2000.10781089

[2] Dalmont, J. P., Nederveen, C. J., Dubos, V, et al. Experimental determination of the equivalent circuit of an open side hole: linear and nonlinear behavior[J], *Acta Acustica united with Acustica*, **88**(4), 567-575, (2002). https://doi.org/10.1134/1.1494032

[3] Ji, Z. L. Acoustic length correction of closed cylindrical side-branched tube[J], *Journal of Sound and Vibration*, **283**(3-5), 1180-1186, (2005). https://doi.org/10.1016/j.jsv.2004.06.044

[4] Chaitanya, P., Munjal, M.L. Effect of wall thickness on the end corrections of the extended inlet and outlet of a double-tuned expansion chamber[J], *Applied Acoustics*, **72**(1), 65-70, (2011). https://doi.org/10.1016/j.apacoust.2010.09.001

[5] Ou-Yang, X. P., Li, L., Fang, X., et al. Research status and prospects of resonant-type hydraulic pulsation attenuators[J], *The Journal of Mechanical Engineering*, **51**(22), 168-175+182, (2015). https://doi.org/10.3901/JME.2015.22.168

[6] Ji, Z. L. *Acoustical theory and Design of mufflers*, Science Press, Beijing, (2015).

[7] Xi, Y., Li, B.R., Gao, L.L., et al. Acoustic attenuation performance prediction and analysis of bladder style hydraulic noise suppressors[J], *Applied Acoustics*, **134**, 131-137, (2018). https://doi.org/10.1016/j.apacoust.2018.01.005

[8] Elnady, T., Abom, M., Allam, S. Modeling perforates in mufflers using two-ports[J], *ASME Journal of Vibration and Acoustics*, **132**(6), 1-11, (2010). https://doi.org/10.1115/1.4001510

[9] Munjal, M. L. *Acoustics of Ducts and Mufflers*, 2nd Edition. John Wiley & Sons Ltd, New York, (2014).

[10] Yang, F., Deng, B. Filtering performance and optimization of double-chamber compound hydraulic attenuators[J], *Proceedings of the Institution of Mechanical Engineers, PartC: Journal of Mechanical Engineering Science*, **232**(18), 3250-3262, (2018). https://doi.org/10.1177/0954406217733293

[11] Yang, F., Deng, B. Fluid acoustic properties of improved hydraulic mufflers with extended necks[J], *International Journal of Acoustics and Vibration*, **24**(4), 638-647, (2019). https://doi.org/10.20855/ijav.2019.24.41327

[12] Yang, F., Deng, B. Pulsation attenuation analysis of double-chamber composite hydraulic suppressors with inserted conical tubes[J], *International Journal of Acoustics and Vibration*, **24**(3), 578-585, (2019). https://doi.org/10.20855/ijav.2019.24.31401

[13] Luo, Z.C. *Fluid network theory*, China Machine Press, Beijing, (1988).

[14] Kenneth, A.M., Elliott, R.G., Kenneth, A.C.. Linear multimodal model for a pressurized gas bladder style hydraulic noise suppressor[J], *International Journal of Fluid Power*, **14**(2), 5-16, (2013). https://doi.org/10.1080/14399776.2013.10781071